CrossMark

Quantification of the blood mixing in the left ventricle using Finite Time Lyapunov Exponents

M. G. Badas · F. Domenichini · G. Querzoli

Abstract Thrombus formation is one of the major complications in myocardial infarction. One of the causes is known to be the regional hemostasis, i.e. the presence of zones where the intraventricular flow is characterised by low stretching of the fluid elements and low mixing. Though Finite Time Lyapunov Exponents (FTLE) have been used both in vivo and in vitro to identify the overall features of cardiovascular flows by means of the Lagrangian Coherent Structures (LCS), they have been introduced in fluid dynamics as descriptors of mixing. Therefore, we investigate the alteration of the intraventricular mixing in an infarcted left ventricle by means of FTLE, looking for the signature of regional hemostasis. The study is carried out on 3D numerical simulations: a ventricle dyskinetic and dilated because of an ischemic pathology is compared to a healthy one and to another with a deviated inlet velocity profile, simulating the presence of a Mechanical Prosthetic Valve in anatomical position. The LCS analysis highlighted the key vortical structures of the flow and their evolution, revealing how they are affected by changes of the ventricle geometry and mobility. Afterwards, the FTLE statistics showed a similar behaviour in the healthy and deviated inlet cases, where hemostasis was not observed, although flow patterns were very different to each other. Conversely, the infarcted ventricle exhibited significantly different values of FTLE statistics, indicating a much lower mixing that is related to the presence of a stagnating region close to the apex. Such differences suggest that FTLE can be considered a potentially useful tool for the characterisation of the mixing properties of the intraventricular flow and, in particular, for the identification of regional hemostasis. Therefore, further investigations are needed to test the sensitivity and specificity of FTLE statistics to the severity of the pathology.

Keywords Left ventricle · Blood mixing · Finite Time Lyapunov Exponents · Lagrangian Coherent Structures

1 Introduction

Vortex formation and evolution in the left ventricle (LV) is acknowledged to be intimately linked to the condition of the heart (see [1] and references therein). Although the hemodynamic picture is still incomplete, there are evidences that the flow in a healthy LV follows some optimization rules for an efficient coupling between diastolic filling and systolic ejection [2–4]. Existing studies recognised a central role to the

M. G. Badas · G. Querzoli (✉)
DICAAR, Università di Cagliari, Cagliari, Italy
e-mail: querzoli@unica.it

F. Domenichini
Dipartimento di Ingegneria Civile e Ambientale,
Università di Firenze, Florence, Italy

formation and evolution of vortex structures inside the LV, whose features were found to be highly sensitive precursors of cardiovascular pathologies [5–7]. Hence, alteration of flow patterns, e.g. due to artificial implants [8, 9] or cardiac diseases, may be considered useful indicators for an early diagnosis. Recent in vivo studies based on Cardiac Magnetic Resonance (CMR) permitted to deepen the LV hemodynamics and to investigate its modification in pathological conditions by the tracing of synthetic particles [10–14]. However, the increasing availability of detailed data demands for the definition of reliable methods of analysis and quantitative indexes yielding simple and clearly readable diagnostic support.

By means of numerical modelling and tracking of synthetic particles we investigate the effectiveness of Finite Time Lyapunov Exponents (FTLE) for the eduction of information about topology of the flow and its mixing characteristics, paying particular attention to the possible thrombus formation in a dyskinetic, dilated LV after regional ischemia. In fact, it is recognised that myocardial infarction may cause regional hemostasis which, in turn, has been related to a high incidence of thrombus formation and rapid growth [15–17].

FTLE were first introduced by Haller [18], and then have been successfully used in different contexts, including biological and geophysical flows [19–21], in order to track vorticity structures and to unveil their connections to energetic and mixing processes. From FTLE, Lagrangian Coherent Structures (LCS), which retain fundamental information about the flow, can be inferred [22]. LCS analysis can be very helpful in cardiovascular fluid dynamics: it permits identification of stagnant fluid areas which increase the risk of thrombus and cause blood cells deterioration. Likewise it is also able to differentiate the regions more directly affected by the vortex presence and possibly their modifications due to pathologies. In the last years, FTLE investigation has been successfully applied also to cardiac fluid dynamics: it was used for the analysis of both numerical simulations [19] and in vitro study [23] of a mechanical heart valve, as well as for the in vitro investigation of vortical structures educed from two-dimensional velocity fields in a LV model [24]. Moreover, FTLE are also becoming popular in the in vivo studies and have been acknowledged as an important method for Lagrangian

analysis of blood transport [25]. This approach has been recently applied to clinical studies of the LV in healthy subjects, and in patients affected by dilated cardiomyopathy: Hendabadi et al. [26] considered both forward and backward FTLE derived from 2D Doppler-echocardiography, while Charonko et al. [27] analyzed forward FTLE fields derived from 2D CMR. Töger et al. [28] focused on backward FTLE fields from 3D CMR intraventricular velocity data, during LV rapid filling. Though FTLE are a powerful tool for the identification of the flow patterns through LCS, they have been originally introduced in fluid dynamics for the description of mixing and stretching of fluid elements [29, 30] in chaotic flows that cannot be considered fully turbulent. This is the typical condition of the intraventricular flow, characterised by the periodic development of large coherent structures, which grow and become unstable during the diastole and vanish almost completely during the systole. As a consequence, FTLE appear to be a very promising diagnostic tool. On one hand they help highlighting the overall structure of the flow; on the other hand they describe the mixing and stretching of the fluid elements, thus the analysis of FTLE probability density function and its evolution throughout the cardiac cycle is a potential indicator of the presence of conditions prone to thrombogenesis.

In the following, after the description of the overall features of the flow by means of the LCS derived from FTLE fields, we show the FTLE statistical analysis in order to highlight mixing properties favourable to thrombus formation in an infarcted ventricle. Three different ventricular conditions are reproduced by computational modelling. The case of dilated cardiomyopathy in presence of dyskinesis as a consequence of myocardial infarction is compared to the flow in a healthy LV, as a reference. An additional comparison is presented, the case mimicking the LV flow due to a mitral valve replacement with a mechanical prosthesis in anatomical orientation. The aim of this latter comparison is differentially testing the proposed analysis against the case of a highly perturbed intraventricular flow, which does not present regional hemostasis. Finally, FTLE analysis is coupled to virtual particle tracking that gives an insight into the role that the vortical structures onset and evolution have on the permanence of blood in the LV.

2 Methods

2.1 Numerical simulation

Blood is assumed to be a Newtonian incompressible fluid, whose motion is driven by the Navier–Stokes and continuity equations:

$$\frac{\partial \vec{v}}{\partial t} + \vec{v} \cdot \nabla \vec{v} = -\frac{1}{\rho}\nabla p + v\nabla^2 \vec{v}, \quad \nabla \cdot \vec{v} = 0, \qquad (1)$$

where t is the time, $\vec{v}$ the velocity, p the pressure, $v = 3.3 \cdot 10^{-6}$ m^2/s the kinematic viscosity and $\rho = 1060$ kg/m^3 the density. The system (1) is solved numerically using an Immersed Boundary Method [31, 32], where the LV boundaries are immersed in a wider computational box (Fig. 1). Simulations are performed imposing the no-slip condition at the chamber wall, whose prescribed motion represents the forcing term of the problem. Velocity profiles are imposed at the mitral and aortic orifices mimicking the in- and out-flow through the mitral and aortic valves, respectively. Although the inherent simplifications, this approach, which does not take into account the valvular dynamics and the active role exerted by the LV tissues, was proven to be able to reproduce the salient features of the observed LV dynamics [8]. The physiological LV is simulated with reference to a typical endocardial shape deduced from a human subject, with no diagnosed cardiac disease, where, in order to reduce variability due to specific geometries, at each instant of the heart cycle the normal LV cavity is approximated as that of half a prolate spheroid [8].

Such a healthy ventricle presents an Ejection Fraction (EF) of 55 %. The mitral inflow is directed into the LV parallel to its long axis. For the simulation of the infarcted LV, the ventricle wall motion is obtained from that of the healthy case reducing the longitudinal and circumferential strain of the anterior and inferior inter-ventricular septum at the median-apical level [33]. This diskinetic region corresponds to a circumferential sector in the range $\pi/2 < \theta < 7\pi/6$ in the lower half of the LV wall, being θ the polar azimuthal coordinate. Specifically, at each instant of time, the healthy strains at the ventricle boundary are multiplied by a reduction coefficient

$$c(\eta, \theta) = 1 - A \exp\left[-\left(\frac{\theta - \theta_c}{2\theta_s}\right)^4 - \left(\frac{\eta - \eta_c}{2\eta_s}\right)^4 \right],$$
$$(2)$$

where the factor A represents the entity of the infarction, η is the spheroidal coordinate along the wall (Fig. 1). θ_c and η_c indicate the centre of the infarcted region, θ_s and η_s are a measure of its extension. Here the value of A was set to 2, which corresponds to a decrease in the EF value down to 32 %. For both the healthy and infarcted cases the mitral jet has an elliptic blunt shape centred in the mitral orifice and directed along the LV main axis. For the third simulation, a 15° inclination of the mitral jet, with respect to the LV axis, is imposed. That condition mimics the typical deviation of the flow after the implantation of a prosthetic mechanical valve (PMV) in anatomical orientation [8]. Figure 2 shows the

Fig. 1 Sketch of the LV model: a vertical section (*left panel*) on the symmetry plane intersecting the centres of the mitral (MO) and aortic (AO) orifices, and the top horizontal view (*right panel*)
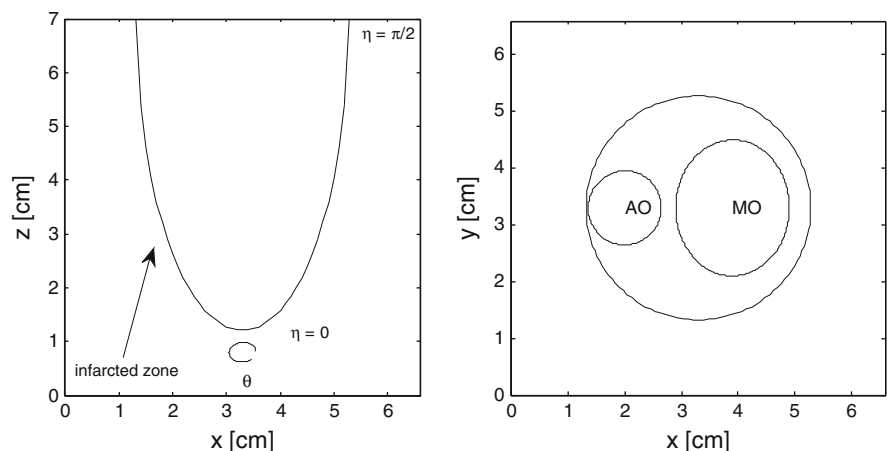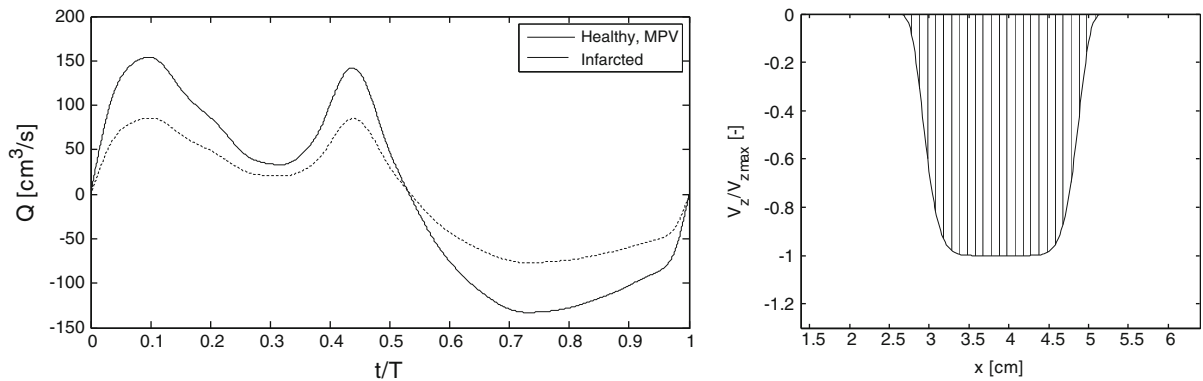
Fig. 2 *Left panel* LV flow rate as a function of non-dimensional time. Positive values: diastole, negative ones: systole. Mitral blunt velocity profile during diastolic phase (*right panel*)

ventricular flow rate as a function of non-dimensional time (right panel), and a long-axis section of the mitral blunt profile entering the mitral orifice (MO) during the diastolic phase (left panel).

From the numerical point of view, the spatial discretisation is based on centred second-order finite differences on a 3D staggered grid; time advancement is performed by a fractional step method, where the prediction is made with an explicit third-order Runge–Kutta scheme for the temporal advancement of the Navier–Stokes equation, and the correction is made by solving the Poisson equation to ensure the continuity constraint [33]. An extensive validation has been performed to assure the correctness of the numerical solution with respect to accuracy and independence of the simulation parameters. Results reported in what follows have been obtained with a computational box $Lx = Ly = 6.6$ cm, $Lz = 7.0$ cm. The computational grid consist of $Nx = Ny = Nz = 128$ nodes, and the time step of integration is $dt = T/1024$. The spatial and temporal resolution has been tuned and checked for accuracy in previous studies of intraventricular flows using the same numerical method [32, 33]. The non-dimensional parameters driving the phenomenon are the Reynolds (Re) and Womersley (Wo) numbers:

$$\text{Re} = \frac{UD}{v}, \qquad Wo = \sqrt{\frac{D^2}{Tv}} \tag{3}$$

where D is the maximum diameter of the ventricle, U the peak velocity through the mitral orifice, T the period of the cardiac cycle. The corresponding values, summarized in Table 1, are within the physiological range.

Table 1 Dimensional and non-dimensional parameters for the three simulated cases

	T (s)	D (cm)	U (cm/s)	Re	Wo
Healthy	1	4.97	45.12	6795	27.4
PMV	1	4.97	47.97	7225	27.4
Infarcted	1	4.97	25.15	3787	27.4

2.2 Finite Time Lyapunov Exponents and Lagrangian Coherent Structures

Finite Time Lyapunov Exponents describe the stretching rate of fluid elements and were initially proposed for the quantification of mixing in chaotic flows [30]. This approach is based on the idea that fluid particles experiencing high stretching are related to regions of good local mixing, and vice versa.

Later, Haller [34, 35] employed FTLE in order to analyze the Lagrangian Coherent Structures that represent a deep signature of the evolving vortex pattern. As a matter of fact, coherent structures in a three dimensional flow are well represented by surfaces where large separation between particles occurs. These surfaces act as pseudo-barriers to transport and mixing, and separate flow regions characterized by different dynamical behaviour.

The FTLE measure the maximum linearised growth rate of the distance among initially adjacent particles tracked over a finite integration time, T_i. In order to perform FTLE computation, the flow map is introduced:

$$\Phi_t^{t+T_i} : x(t) \rightarrow x(t + T_i), \tag{4}$$

where $\Phi_t^{t+T_i}$ maps a material point $x(t)$ at time t to its position at time $t + T_i$, therefore embedding the Lagrangian description of fluid motion. After linearization, the amount of stretching of particles can be defined in terms of the finite-time Cauchy–Green deformation tensor:

$$\Delta = \left(\frac{d\Phi_t^{t+T_i}(x)}{dx} \right)^2, \tag{5}$$

where $\frac{d\Phi_t^{t+T_i}(x)}{dx}$ is the deformation gradient. Thus, the FTLE, $\sigma(x; t; T_i)$, are defined as:

$$\sigma(x, t, T_i) = \frac{1}{|T_i|} \ln \sqrt{\lambda_{\max}} \tag{6}$$

being $\lambda_{\max}$ the maximum eigenvalue of Δ and $\sqrt{\lambda_{\max}}$ corresponds to the maximum stretching factor. Eigenvalues higher than unity are found for particles that separate in time, and smaller than unity when they converge. Those trajectories can be evaluated either forward or backward in time. For positive T_i values, the FTLE measure separation forward in time, thus unveiling the so-called repelling structures; conversely, when a negative T_i value is used, the FTLE measure separation backward in time, thus highlighting attracting structures. The joint analysis of backward and forward FTLE is a powerful tool for the identification of regions enclosing vortices. Depending on the T_i, different details in the FTLE structure are revealed, and the choice of an appropriate value for T_i is strictly connected to the relevant time scales of the flow. For each of the three analysed ventricle conditions, we chose an integration time, T_i, equal to the advection time scale defined as the ratio between the end-diastolic ventricle diameter and the peak mitral velocity, U. This results in $T_i/T = 0.12$ for the healthy ventricle and the deviated inflow, and $T_i/T = 0.22$ for the infarcted ventricle, where T is the period of the cardiac cycle. The FTLE computation has been performed on the 3D numerical velocity fields using the public domain code NEWMAN [36].

LCS are generally identified through the locally maximizing surfaces, or ridges, of the FTLE field. Given a generic scalar function $f \subset \Re^N$, its ridges are characterized as a set of points where f is maximized in $p < N$ independent directions, thus forming a set of dimension $n = N - p$. According to the height ridge definition [37], ridges are computed from the eigenvectors of the Hessian matrix $H = \nabla^2 f$ associated with the p smallest eigenvalues $\lambda_1 < \cdots < \lambda_p$ of H itself, provided that these eigenvalues are negative. Spurious structures can be then filtered out based on the value of f and of the crease strength $|\lambda_p|$.

Actually, caution has to be exercised when inferring LCS from FTLE fields, since, as pointed out by [38, 39], a ridge in the FTLE field may highlight a shear LCS or indicate absence of LCS at all [38, 39]. Nonetheless, ridges in the FTLE fields have been extensively adopted as a footprint of the LCS of the flow. The FTLE approach to LCS detection is typically heuristic: a LCS straightforward identification by means of a visual inspection and an appropriate thresholding of FTLE fields is generally used. In the following, three-dimensional LCS are identified by the algorithm developed by Schultz et al. [40], which is a voxel based ridge surface extraction method that includes a set of topological principles to improve both correctness and performance, and to avoid subjectiveness.

2.3 Particle traces

In order to complement the FTLE analysis, the trajectories of a number of fluid particles entering the ventricle through the mitral orifice during the LV filling were numerically calculated. This was aimed to further clarify the role of LCS, thanks to the superposition of the particle positions and FTLE maps, and to verify how LCS act as pseudo-barriers for transport and mixing. Moreover, particle traces themselves were analyzed to evaluate the different components of the ventricular flow.

Around 1400 particles, with a random uniform spatial distribution on the mitral orifice plane, were emitted during each time step of the diastole, and were subsequently tracked during the two following cardiac cycles. As a result, for each of the examined cases, a total amount of about 800,000 particles was simulated. This set of samples can be considered as well representative of the ventricular inflow, being of the same order of magnitude of the 3D grid employed in the numerical simulations.

Particles were then divided into separated sets in order to quantify the residence time of the blood in the LV by means of the evaluation of the flow components. These are defined as: Direct Flow (DF, particles

that enter the LV during the single diastolic filling and that leave the LV during the first following systole); Delayed Ejection Flow (DEF, particles remaining in the LV during the first systole, and exiting at the following, second systolic ejection); Retained Flow (RF, particles that do not leave the ventricle during the two analyzed heart beats, and that therefore has a residence time greater than two heartbeats).

This Lagrangian approach which differs from the Eulerian formulation proposed by Mangual et al. [41] since it does not include the effects of diffusion. However it was preferred in the present study since it emulates the way typically followed in vivo with CMR data [10–13], despite some small differences in the flow component definition.

3 Results

3.1 FTLE and LCS

Three-dimensional views of FTLE ridges, at selected time instants, are reported in Figs. 3, 4 and 5 for the three conditions. Representations are cut on the symmetry, vertical plane intersecting the centres of the mitral and aortic orifices. LCS are identified by the unsupervised algorithm developed by Schultz et al. [40]. Relation between inflow and LCS is shown by superimposing the positions of the particles released from the mitral orifice during the diastole. Particles entering the ventricle during the early filling E-wave are represented by green dots, while particles released during the A-wave are yellow. The inset in the low left corner of each plot shows the point in the flow-rate cycle.

For the healthy ventricle, LCS clearly describe the main features of the diastolic flow, i.e. the growth and evolution of the vortex ring during the E-wave (Fig. 3a, d), which leads to the generation of a clockwise vortical structure dominating most of the ventricle at the end of the diastole (Fig. 3b, e) [2, 3, 42, 43]. The weaker secondary structure generated by the A-wave can be easily recognised in Fig. 3b. Attracting LCS identify the front of diastolic jet, sharply separating the fluid which just entered the ventricle from the receiving fluid. LCS plots at the systolic peak (Fig. 3c, f) show that the structures generated during the diastole penetrated down to the apical region and involve most of the ventricular volume.

The completely different flow field due to the deviation of the mitral jet, which simulates the presence of a mechanical prosthetic valve, can be observed in Fig. 4a, d. In that case the counter-clockwise branch, on the right part of the plots, increases in size. At the same time, the clockwise branch of the vortex tends to vanish due to the interaction with the opposite (posterior) wall. As a result, a counter-clockwise rolling LCS dominates the intraventricular flow at the end of the diastole (Fig. 4b, e). Similarly to the healthy case, at the end of the diastole the LCS reaches the apical region, thus involving the whole ventricular chamber at the systolic peak (Fig. 4c, f). A different scenario is depicted in Fig. 5, where the infarcted case is reported. The presence of the apical akinetic region is related to a weaker, less intense diastolic jet. The filling flow is not able to propagate beyond the half ventricle length. The first vorticity structure, associated with the E-wave inflow, is smaller and weaker than that detected in the healthy case, Fig. 5a, d. At the end of the diastolic phase, the first and secondary structures are almost completely merged. Their interaction leads to the loss of their coherence, (Fig. 5b, e). No significant LCS are present in the apical region, where the flow is almost irrotational at the systolic peak (Fig. 5c, f).

Three-dimensional plots reported above show the overall structure of the LCS. However, further details can be educed by the analysis of the two-dimensional FTLE maps. Figures 6, 7 and 8 show colour maps of the FTLE distribution on the vertical symmetry plane passing through the LV apex and across the centres of both the mitral and aortic orifices. Maps are plotted at the same time instants as above. Corresponding velocity fields are superimposed. The small inset in the low left corner of each plot shows the point in the flow-rate cycle.

Ridges characterising the LCS are apparent on the maps, confirming that FTLE are an effective tool for the analysis of the structure of the intraventricular flow [24]. At the end of the E-wave the coherent vortex ring trapping the fluid just entered from the mitral orifice is formed, and, on the vertical section, it is represented by a pair of counter-rotating vortices. The propagation front of the structure is highlighted by the backward FTLE (Figs. 6, 7, 8, panel a), whereas forward FTLE show the trailing boundary of the inflow (Figs. 6, 7, 8, panel d). In the healthy ventricle the left dominant vortex occupies the central region of the plane,
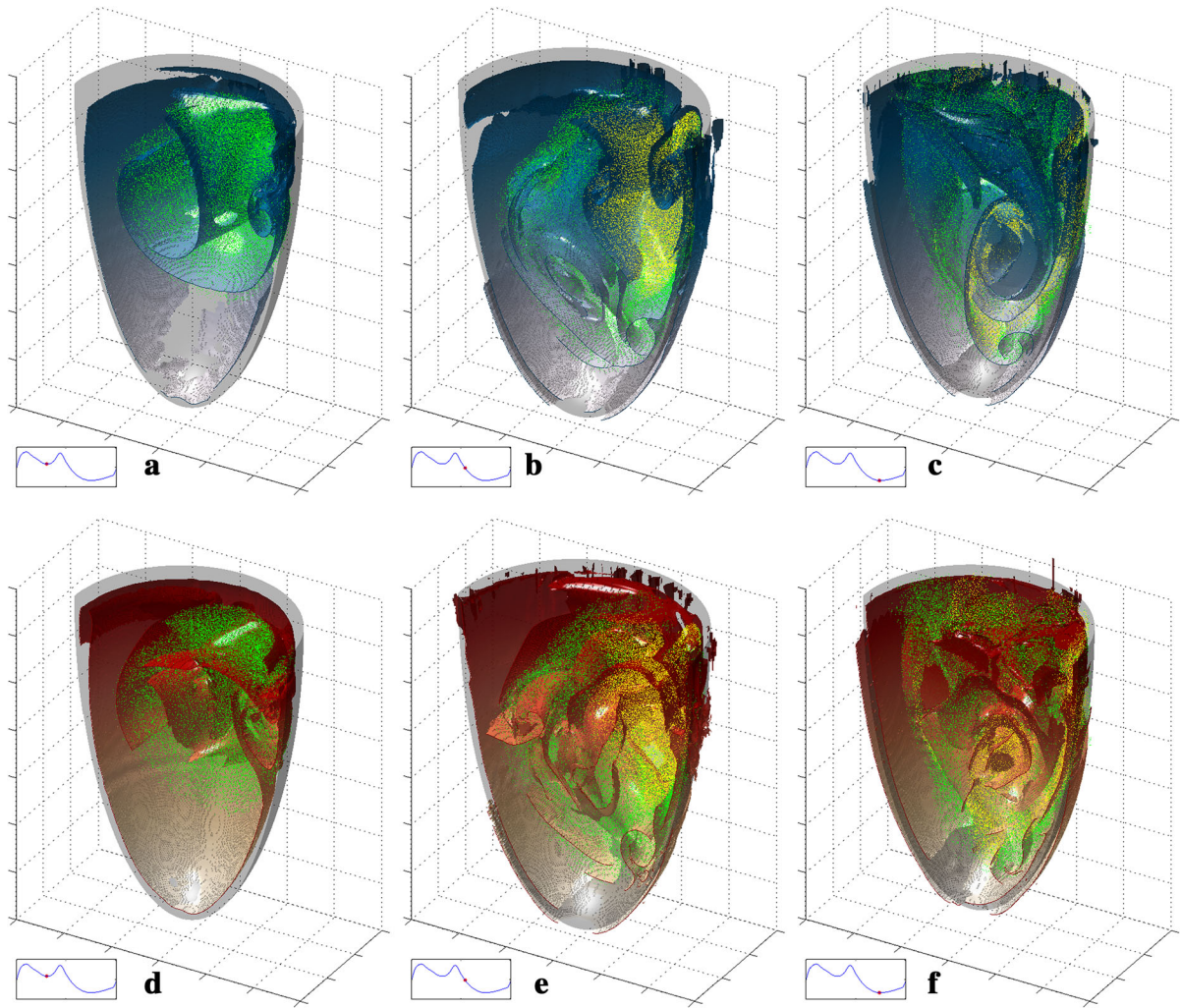
Fig. 3 Three-dimensional LCS in the healthy ventricle sectioned by the vertical symmetry plane intersecting mitral and aortic centres at three instants of the cardiac cycle: t = 0.30 T (diastasis), *left column*: t = 0.54 T (end of diastole), *centre column*: t = 0.73 T (mid systole), *right column*. Attracting LCS are displayed in bluish, repelling LCS in reddish. *Green dots* are particles released from the mitral orifice during the E-wave; *yellow dots* are particles released during A-wave. (Color figure online)

Fig. 6a, moving toward the posterior wall (right of the plot), Fig. 6b. On the opposite, in the MPV case the dominant right vortex moves toward the opposite (anterior) wall, Fig. 7b. In the infarcted ventricle the inflow travelled a significantly lower distance compared to the previous cases, resulting in a more symmetric vorticity structure (Fig. 8a). This is due to the reduced wall contractility prescribed to model the ischemia; the presence of the akinetic region close to the apex can be observed in the left part of the figure.

At the end of the diastolic filling, just before the ejection, the interaction between the structure generated by the E-wave and the vortex ring resulting from the A-wave can be observed (Figs. 6, 7, 8, panels b, e). In the healthy case, the vorticity arrangement leads to the creation of channel redirecting the flow towards the outflow path (Fig. 6b, e) as documented in vitro by Fortini et al. [42]. This phenomenon is not present in the case of the MPV deviated jet (Fig. 7b, e), as far as the A-wave vortex is interacting with the E-wave structure and the flow is characterised by a reversed circulation, which does not facilitate the following systolic ejection [8, 9]. Notwithstanding the completely different resulting
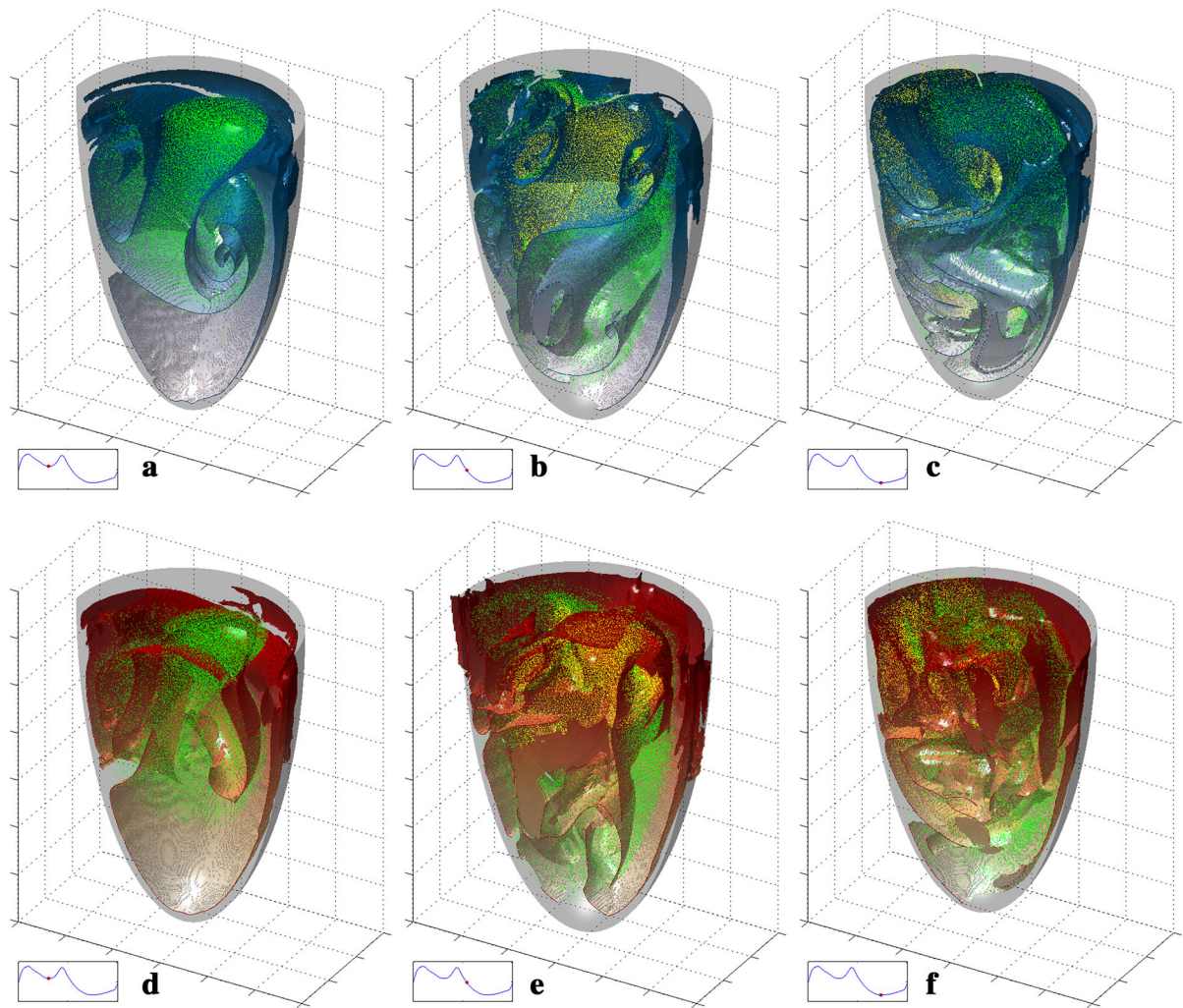
Fig. 4 Three-dimensional LCS in the ventricle with the deviated inflow simulating the implantation of a MPV sectioned by the vertical symmetry plane intersecting mitral and aortic centres at three instants of the cardiac cycle: t = 0.30 T (diastasis), left column: t = 0.54 T (end of diastole) *centre column*: t = 0.73 T (mid systole) *right column*. Attracting LCS are displayed in bluish, repelling LCS in reddish. *Green dots* are particles released from the mitral orifice during the E-wave; *yellow dots* are particles released during A-wave. (Color figure online)

flow pattern, in both healthy and MPV cases the structures generated during the diastole propagate down to the apical region (Figs. 6, 7, panels c, f). Conversely, in the infarcted ventricle (Fig. 8), the A-wave vortex ring slowly interacts with the E-wave structure, and it is confirmed that the diastolic structures remain confined in the upper part of the ventricle (Fig. 8, panels c, e). The presence of a zone of virtually quiescent fluid in the apical region of the LV observed in the velocity vectors maps of Fig. 8 during the whole cycle is a clear indication of regional hemostasis in the infarcted LV.

3.2 FTLE statistics

Formation of thrombi after myocardial infarct is known to be correlated to anomalies in the intraventricular flow patterns [16] and, in particular, to the presence of regional hemostasis. FTLE describe the separation rate of fluid particles, and can be considered a measure of stretching of fluid elements and mixing. Consequently, their statistics are here analysed with the aim of revealing conditions of potential thrombogenesis. Gaussian probability density functions (PDFs) of FTLE are characteristic of homogeneous mixing,
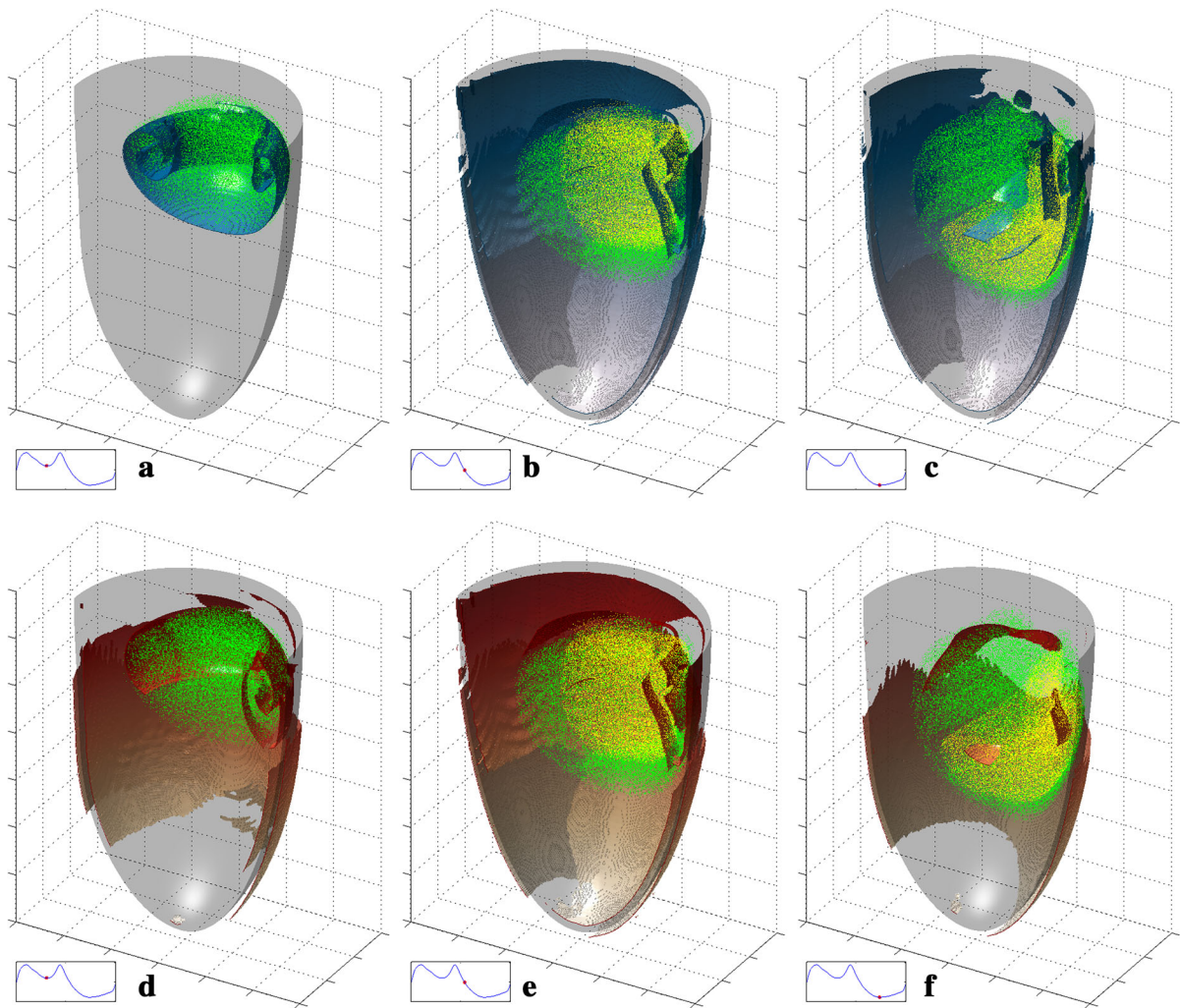
Fig. 5 Three-dimensional LCS in the infarcted ventricle sectioned by the vertical symmetry plane intersecting mitral and aortic centres at three instants of the cardiac cycle: t = 0.30 T (diastasis), *left column*: t = 0.54 T (end of diastole) *centre column*: t = 0.73 T (mid systole) *right column*. Attracting LCS are displayed in bluish, repelling LCS in reddish. *Green dots* are synthetic particles released from the mitral orifice during the E-wave; *yellow dots* are particles released during A-wave. (Color figure online)

where the trajectories of fluid particles randomly map the entire domain, whilst in case of heterogeneous mixing, the PDFs are not-Gaussian, with broader and, possibly, more asymmetric distributions with increasing degree of heterogeneity [44]. We focus on forward FTLE PDFs at the same characteristic time instants of the heartbeat considered above (Fig. 9), to then analyze their statistics and time evolution throughout the whole cardiac cycle (Fig. 10).

Panels in Fig. 9 show that at end of E-wave (left column) the FTLE PDFs for the three cases are positively skewed. The healthy and MPV distributions

appear to be quite similar. Their shape is almost bimodal, indicating that two well defined regions with different mixing properties are simultaneously present within the LV. On the opposite, the infarcted LV presents a sharp peak at lower values of the FTLE, associated to the large part of the LV which is not directly affected by the diastolic inflow. An almost undistinguishable thin, positive tail indicates the presence of a single, localized structure producing mixing. When PDFs are computed at the end of the A-wave (centre column), the first two LV conditions still look very similar: the distributions are still
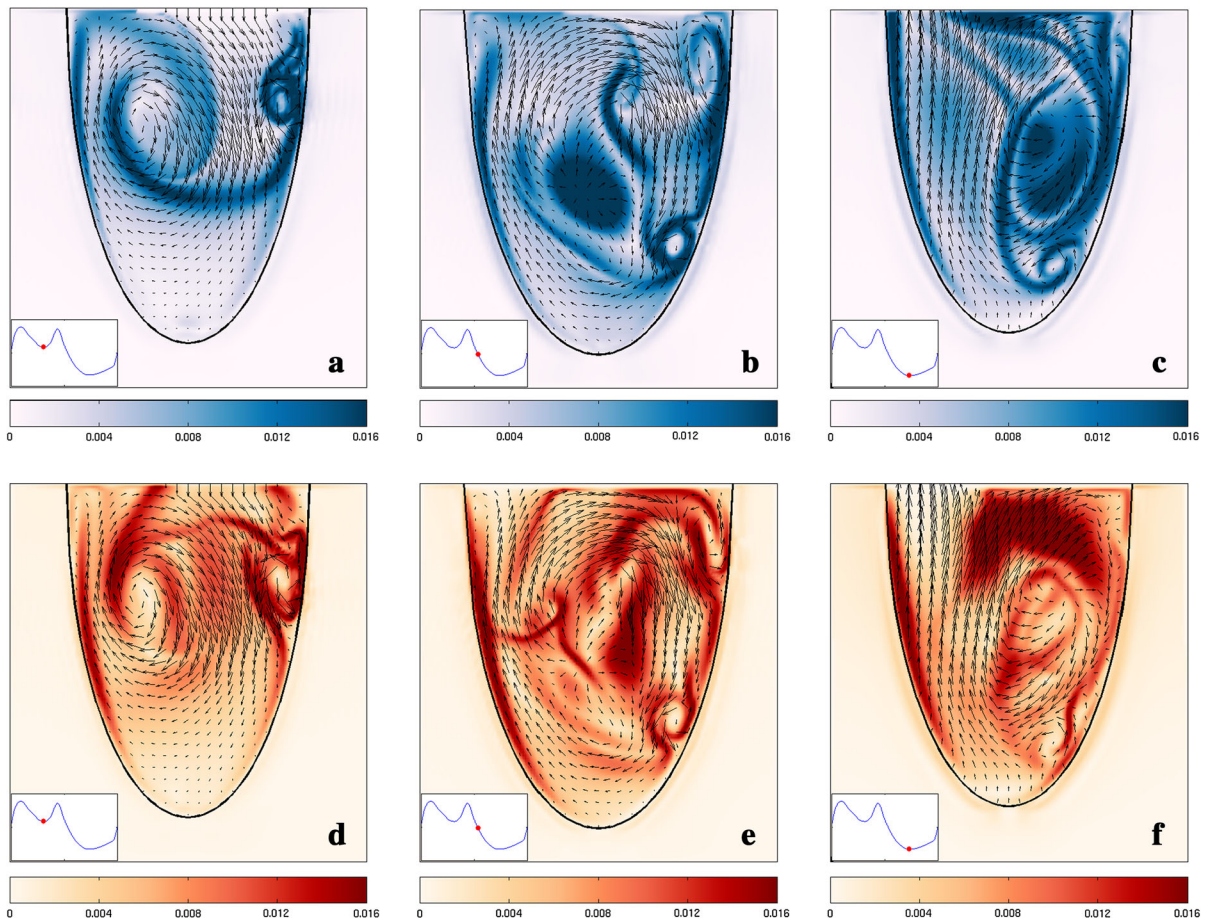
Fig. 6 FTLE maps in the healthy ventricle at instants of the cardiac cycle: t = 0.30 T, *left column*: t = 0.54 T, *centre column*: t = 0.73 T, *right column*. Backward-time FTLE are displayed in bluish (*top row*), forward-time ones in reddish (*bottom row*). (Color figure online)

positively skewed but broader and less peaked, due to the increasing complexity of the flow, which characterises the whole ventricular chamber. The PDF for the infarcted LV shows a very different picture, being still shrunk and shifted to the lower values, indicating very low level of mixing. This is due to the fact that the two vortex rings produced during diastole in the case of infarcted ventricle coalesce into a single, compact structure, whilst in the other two conditions they remain separate, and their motion involves also the apical region with a more widespread mixing. At the systolic peak (right column), healthy and MPV cases present a broader and more Gaussian distribution, due to the disruption of the vortex structure, which causes a more homogeneous mixing. On the contrary, the PDF in the infarcted LV case suggests a highly

heterogeneous mixing, due to the permanence of the single vortex structure during the beginning of the systolic phase. The time evolution of the mean, standard deviation and skewness of the forward FTLE distribution over the whole ventricle volume are presented in Fig. 10. The mean values have very similar trends in healthy and MPV deviated ventricles, with slightly lower values for the healthy condition (Fig. 10, top panel). Such a difference can be related to the less organised flow promoted by the deviated inflow, which leads to a higher degree of instability. The mean FTLE value increases more steeply at the beginning of the diastole, with a slower growth during the A-wave, followed by the systolic decrease. This is slow at the beginning, and then becomes steeper during the final phase of the systole, when the vortical
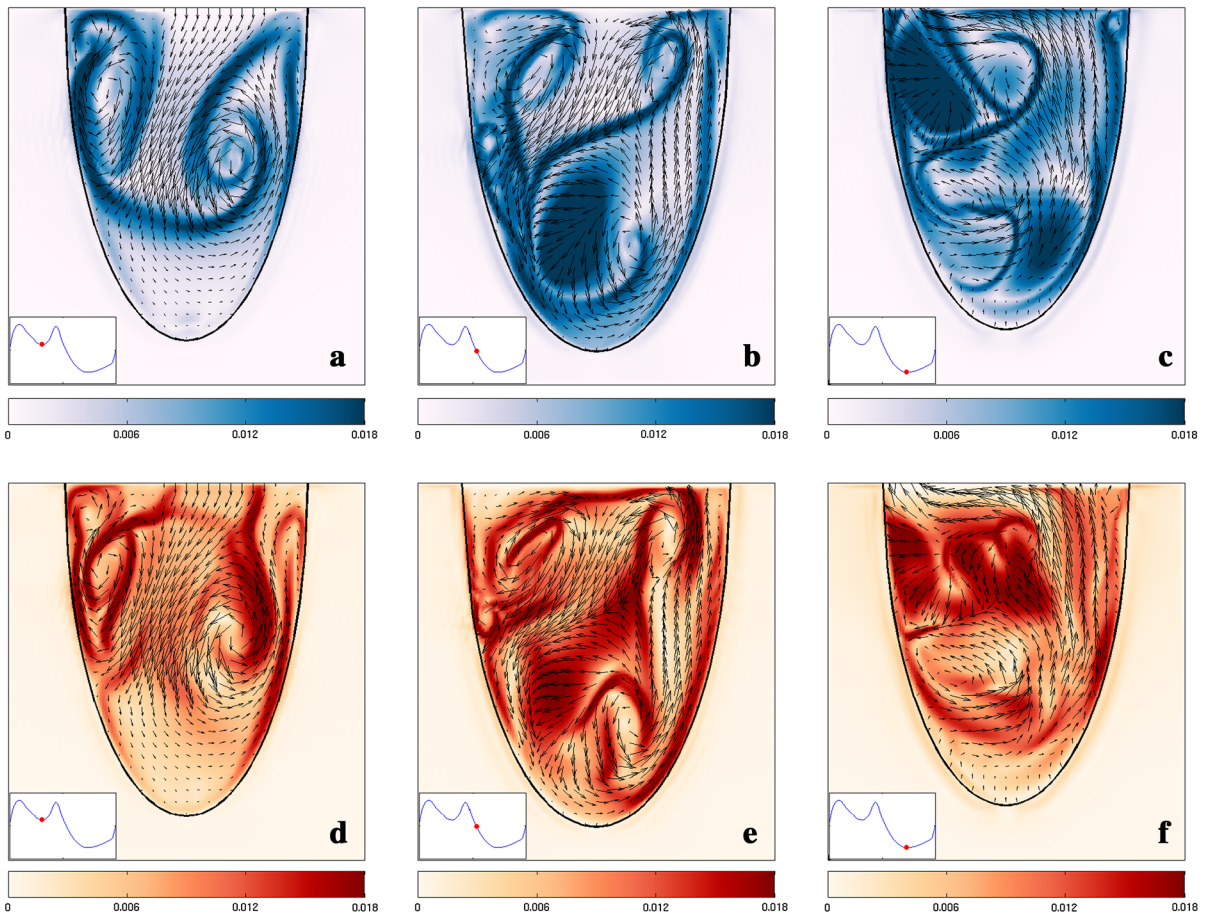
Fig. 7 FTLE maps in the ventricle with deviated inflow resembling MPV implantation at three instants of the cardiac cycle: t = 0.30 T, *left column*: t = 0.54 T, *centre column*: t = 0.73 T, *right column*. Backward-time FTLE are displayed in bluish (*top row*), forward-time ones in reddish (*bottom row*). (Color figure online)

structures generated during the diastole vanish and the flow is dominated by the acceleration toward the aortic orifice. The dyskinetic, dilated case yields much lower mean FTLE values during the whole cycle. Moreover, mean FTLE is nearly constant during the heartbeat, and the sudden increase corresponding to the onset of the E-wave vortex ring that is observed in the other cases does not occur. These lower values are due to the contribution of the apical region that is not reached by the diastolic vorticity structures, resulting in constantly small values of FTLE. The standard deviation of FTLE distribution (mid panel of Fig. 10) can be regarded as a measure of the amplitude of the range of mixing scales within the ventricular volume. In the normokinetic ventricles, the maximum value is attained at the first diastolic peak, when the ventricular flow is characterised by zones with significantly

different flow features, that is an upper portion where a single vortex structure is fully developed, and the apical region where the flow is almost irrotational. Both of these cases show much higher values compared to the infarcted case, where the weakness of diastolic jet does not allow the development of large coherent structures. This is confirmed by the analysis of the bottom panel of Fig. 10. The skewness is about three times higher in the case of infarcted ventricle than in the normokinetic ventricles. The high, positive skewness indicates that mixing is driven by few, localised events, while most particles experience long separation times. The skewness is particularly high during the development of the diastolic structures, which involves only a small portion of the LV, while the peak of the PDF at low FTLE values is related to a the largest portion of the ventricle, which is not
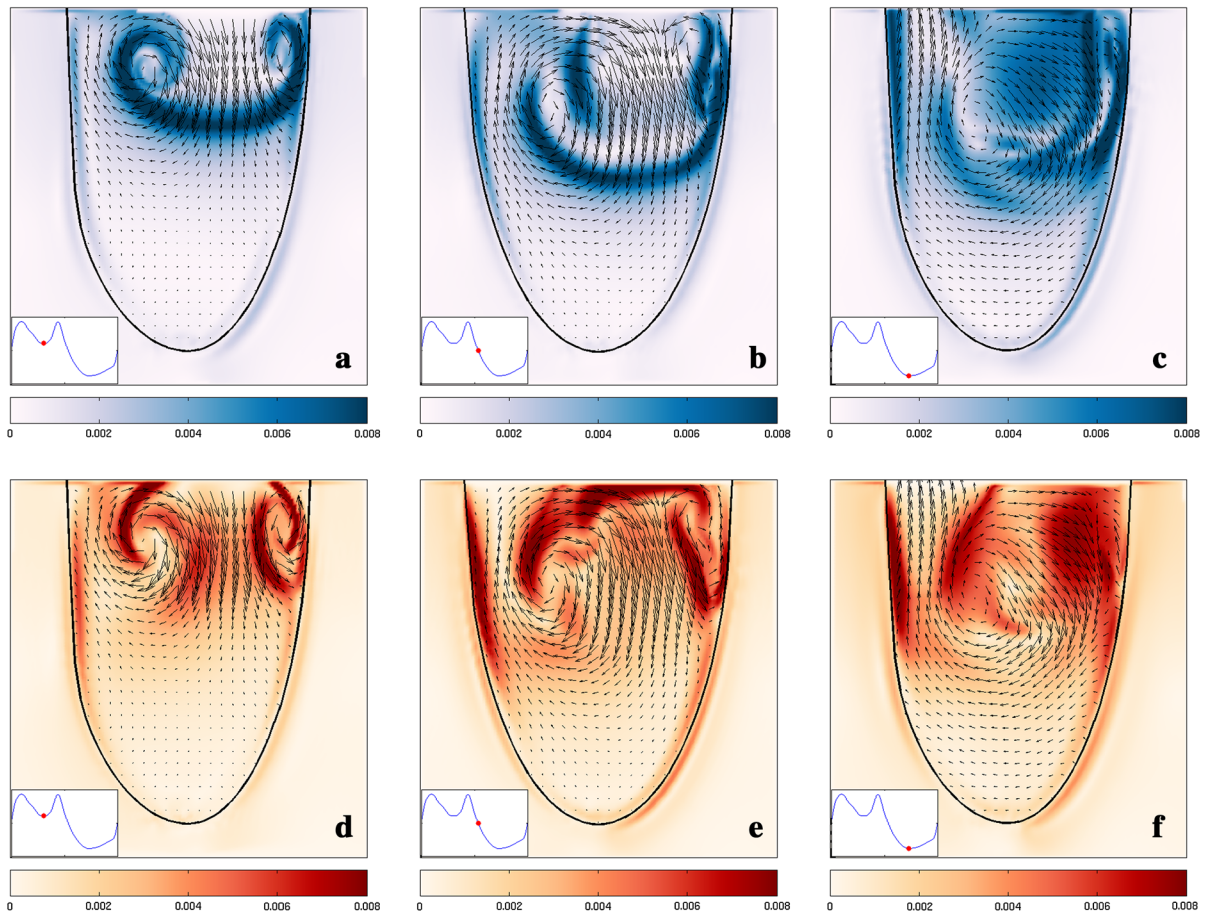
Fig. 8 FTLE maps in the infarcted ventricle at three instants of the cardiac cycle: t = 0.30 T, *left column*: t = 0.54 T, *central column*: t = 0.73 T, *right column*. Backward-time FTLE are displayed in bluish (*top row*), forward-time ones in reddish (*bottom row*). (Color figure online)

involved in significant mixing phenomena and therefore can be related to regional hemostasis (Fig. 9, left column, bottom row).

3.3 Inflow components

The three flow components DF, DEF, and RF are reported in Fig. 11 as fractions of the total incoming flow. In both the normal and the MPV deviated case, the DF is around 50 %. About 83 % of the incoming flow is reached when the DEF is added, while only <20 % of the blood is retained for more than two cycles (RF). Conversely, in the case of infarcted ventricle, the DF component is very small (around 15 %) and the RF is almost the 40 % of the total inflow. The differences between the normal and MPV deviated case become more noticeable when

we track fluid entering the ventricle during the E-wave and A-wave separately (plotted with lighter and darker colours, respectively). The slightly higher DF observed for the MPV deviated inlet is mainly due to the A-wave flow. As a matter of fact, the A-wave particles mainly constitute DEF in the healthy ventricle, whereas DF is the major component for the MPV deviated inlet. The different distribution of the flow components is a consequence of a distinct formation and evolution of the coherent structures: A-wave particles follow the E-flow in the healthy ventricle, while they partly set in front of the E-flow in the deviated case. Though the considered cases are different, these results are qualitatively in agreement with the in vivo 4D CMR measurements in case of dilated cardiomyopathy [10].
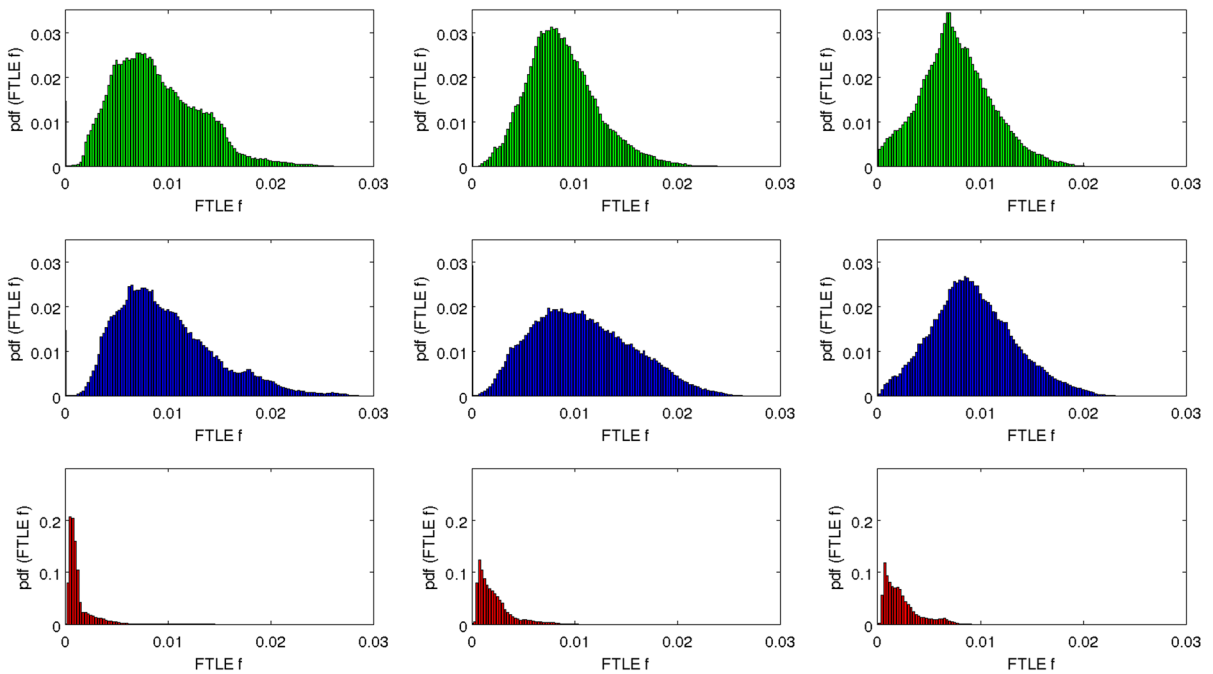
Fig. 9 PDF of forward FTLE computed at characteristic instants of the cardiac cycle: end of E-wave (t = 0.30 T, *left column*); end of A-wave tree analyzed cases: healthy ventricle (*top row*), MPV deviated inflow (*middle row*), cardiomyopathy (*bottom row*)

4 Discussion

Three test cases have been considered: a healthy ventricle, the case of the inflow deviated by the implantation of a mechanical prosthetic valve, and a dyskinetic, dilated ventricle after a myocardial ischemia. Three-dimensional FTLE fields (Figs. 3, 4, 5) were able to reveal the LV coherent structures, also thanks to the application of an unsupervised algorithm for ridge extraction. Detailed analysis of the two-dimensional maps shows that the flow patterns in the healthy and MPV deviated inflow are very different to each other, leading to different partitions of flow components (Fig. 11). However, in both cases the vortical structures generated during the diastole involve the whole ventricular volume during their evolution (Figs. 6, 7) and no persistent regional hemostasis is observed. Conversely, signature of hemostasis is found in the infarcted case, where a compact structure is generated that does not propagated to the apical portion of the LV (Fig. 8). This condition is known to be prone to mural thrombus formation that is one of the principal complications of myocardial infarct.

Typically, these thrombi are characterised by a fast growth and are a potential cause of systemic embolisation [15].

Given that forward FTLE are a measure of the stretching of fluid elements, their statistics have been analysed to look for the signature of hemostasis (Figs. 9, 10). Comparison of mean, standard deviation and skewness shows that the two normokinetic LV exhibit values and time evolution quite similar to each other, though they are characterised by very different flow patterns. Conversely, both of them significantly differ from the statistics shown by the infarcted LV, where hemostasis was observed. As a matter of fact, the infarcted ventricle, exhibits mean and standard deviation of FTLE values much lower than the other two cases. For instance, average forward FTLE over the whole cycle of healthy and MVP case is 5.1 and 4.4 times larger than in infarcted LV, respectively. Differently, the skewness of FTLE distribution is about the same and much lower in the two normokinetic cases compared to the infarcted LV. Lower mean value and higher skewness characterising the infarcted ventricle suggest that intense phenomena is limited to a small portion

Fig. 10 Time evolution of the statistics of forward FTLE distribution over the ventricle volume. *Top panel* mean value FTLE; *middle panel* standard deviation of FTLE; *bottom panel* skewness of FTLE
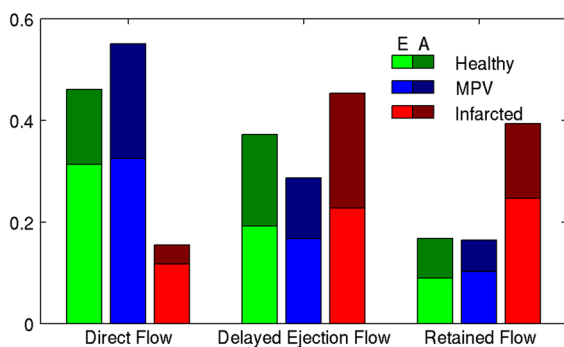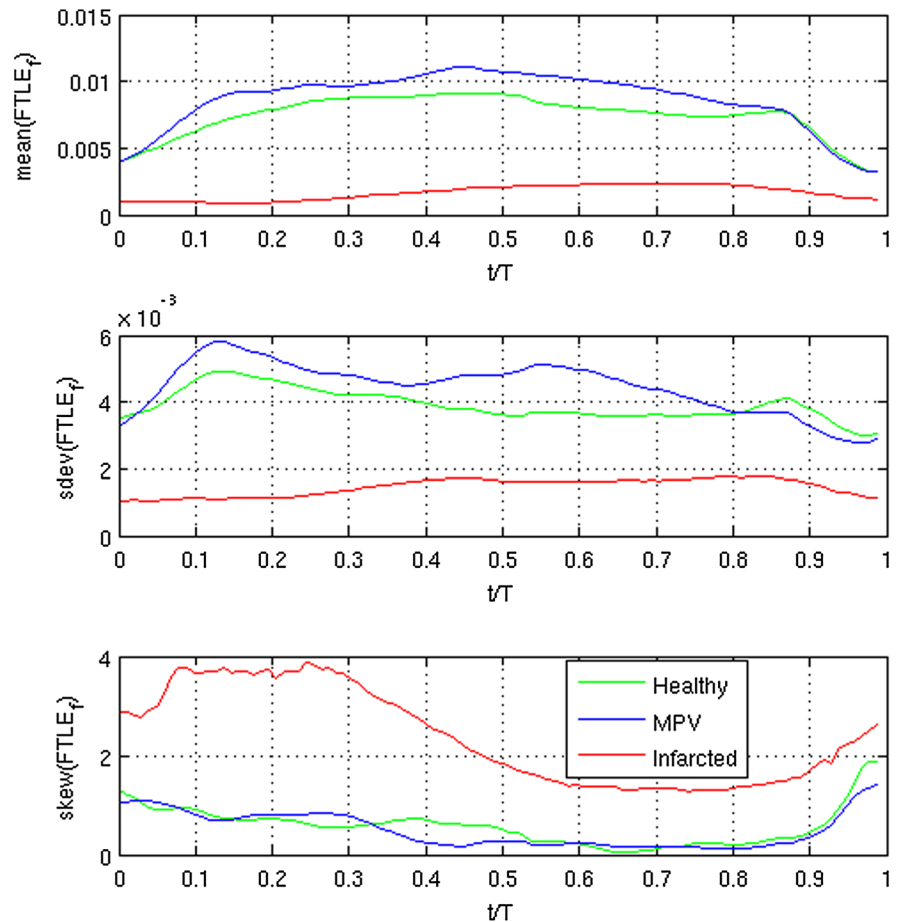

Fig. 11 Distribution of flow components for the total incoming flow and the three ventricle conditions. Each component is subdivided into the E-wave and A-wave contributes (*lighter and darker colours*, respectively). *Green* healthy ventricle. *Blue* MPV deviated inlet. *Red* infarcted ventricle. (Color figure online)

of the LV, whereas most of the ventricular volume is not affected by high stretching rates, depicting the typical features of hemostasis. The result is in

agreement with the velocity vector maps (Fig. 8), which reveal the presence of a portion of nearly quiescent fluid in the apical region.

In conclusion, LCS analysis was able to give a detailed picture of the intraventricular flow structure. Additionally, the significant differences in FTLE statistics observed in the infarcted test case suggest that FTLE analysis is a promising tool for the characterisation of the mixing properties of the intraventricular flow and, in particular, for the identification of regional hemostasis. From the present results stems the need for further clinical studies and or simulations to assess sensitivity and specificity of the FTLE statistics in a wide spectrum of pathologic severity.

References

1. Kheradvar A, Pedrizzetti G (2012) Vortex formation in the cardiovascular system. Springer, London

2. Kilner PJ, Yang GZ, Wilkes AJ et al (2000) Asymmetric redirection of flow through the heart. Nature 404:759–761. doi:10.1038/35008075

3. Pedrizzetti G, Domenichini F (2005) Nature optimizes the swirling flow in the human left ventricle. Phys Rev Lett 95:108101

4. Pierrakos O, Vlachos PP (2006) The effect of vortex formation on left ventricular filling and mitral valve efficiency. J Biomech Eng 128:527–539. doi:10.1115/1.2205863

5. Gharib M, Rambod E, Kheradvar A et al (2006) Optimal vortex formation as an index of cardiac health. Proc Natl Acad Sci USA 103:6305–6308. doi:10.1073/pnas.0600520103

6. Hong G-R, Pedrizzetti G, Tonti G et al (2008) Characterization and quantification of vortex flow in the human left ventricle by contrast echocardiography using vector particle image velocimetry. J Am Coll Cardiovasc Imaging 1:705–717. doi:10.1016/j.jcmg.2008.06.008

7. Sengupta PP, Khandheria BK, Korinek J et al (2007) Left ventricular isovolumic flow sequence during sinus and paced rhythms: new insights from use of high-resolution Doppler and ultrasonic digital particle imaging velocimetry. J Am Coll Cardiol 49:899–908. doi:10.1016/j.jacc.2006.07.075

8. Pedrizzetti G, Domenichini F, Tonti G (2010) On the left ventricular vortex reversal after mitral valve replacement. Ann Biomed Eng 38:769–773. doi:10.1007/s10439-010-9928-2

9. Querzoli G, Fortini S, Cenedese A (2010) Effect of the prosthetic mitral valve on vortex dynamics and turbulence of the left ventricular flow. Phys Fluids (1994–present) 22:041901. doi:10.1063/1.3371720

10. Bolger AF, Heiberg E, Karlsson M et al (2007) Transit of blood flow through the human left ventricle mapped by cardiovascular magnetic resonance. J Cardiovasc Magn Reson 9:741–747. doi:10.1080/10976640701544530

11. Carlhäll CJ, Bolger A (2010) Passing strange flow in the failing ventricle. Circ Heart Fail 3:326–331. doi:10.1161/CIRCHEARTFAILURE.109.911867

12. Eriksson J, Carlhäll CJ, Dyverfeldt P et al (2010) Semi-automatic quantification of 4D left ventricular blood flow. J Cardiovasc Magn Reson 12:9. doi:10.1186/1532-429X-12-9

13. Markl M, Kilner PJ, Ebbers T (2011) Comprehensive 4D velocity mapping of the heart and great vessels by cardiovascular magnetic resonance. J Cardiovasc Magn Reson. doi:10.1186/1532-429X-13-7

14. Töger J, Carlsson M, Söderlind G et al (2011) Volume tracking: a new method for quantitative assessment and visualization of intracardiac blood flow from three-dimensional, time-resolved, three-component magnetic resonance velocity mapping. BMC Med Imaging 11:10. doi:10.1186/1471-2342-11-10

15. Beppu S, Izumi S, Miyatake K et al (1988) Abnormal blood pathways in left ventricular cavity in acute myocardial infarction. Experimental observations with special reference to regional wall motion abnormality and hemostasis. Circulation 78:157–164. doi:10.1161/01.CIR.78.1.157

16. Lu J, Li W, Zhong Y et al (2012) Intuitive visualization and quantification of intraventricular convection in acute ischemic left ventricular failure during early diastole using color Doppler-based echocardiographic vector flow mapping. Int J Cardiovasc Imaging 28:1035–1047. doi:10.1007/s10554-011-9932-0

17. Cordero CD, Rossini L, Martinez-Legazpi P et al (2015) Prediction of intraventricular thrombosis by quantitative imaging of stasis: a pilot color-Doppler study in patients with acute myocardial infarction. J Am Coll Cardiol. doi:10.1016/S0735-1097(15)61310-9

18. Haller G (2001) Lagrangian structures and the rate of strain in a partition of two-dimensional turbulence. Phys Fluids (1994–present) 13:3365–3385. doi:10.1063/1.1403336

19. Shadden SC, Lekien F, Marsden JE (2005) Definition and properties of Lagrangian coherent structures from finite-time Lyapunov exponents in two-dimensional aperiodic flows. Phys D 212:271–304. doi:10.1016/j.physd.2005.10.007

20. Shadden SC, Astorino M, Gerbeau J-F (2010) Computational analysis of an aortic valve jet with Lagrangian coherent structures. Chaos: an Interdisciplinary. J Nonlinear Sci 20:017512. doi:10.1063/1.3272780

21. Badas MG, Querzoli G (2011) Spatial structures and scaling in the Convective Boundary Layer. Exp Fluids 50:1093–1107. doi:10.1007/s00348-010-1020-z

22. Haller G (2015) Lagrangian coherent structures. Annu Rev Fluid Mech 47:137–162. doi:10.1146/annurev-fluid-010313-141322

23. Miron P, Vétel J, Garon A (2014) On the use of the finite-time Lyapunov exponent to reveal complex flow physics in the wake of a mechanical valve. Exp Fluids 55:1–15. doi:10.1007/s00348-014-1814-5

24. Espa S, Badas MG, Fortini S et al (2012) A Lagrangian investigation of the flow inside the left ventricle. Eur J Mech B Fluids 35:9–19. doi:10.1016/j.euromechflu.2012.01.015

25. Bermejo J, Benito Y, Alhama M et al (2014) Intraventricular vortex properties in nonischemic dilated cardiomyopathy. Am J Physiol Heart Circ Physiol 306:H718–H729. doi:10.1152/ajpheart.00697.2013

26. Hendabadi S, Bermejo J, Benito Y et al (2013) Topology of blood transport in the human left ventricle by novel processing of Doppler echocardiography. Ann Biomed Eng 41:2603–2616. doi:10.1007/s10439-013-0853-z

27. Charonko JJ, Kumar R, Stewart K et al (2013) Vortices formed on the mitral valve tips aid normal left ventricular filling. Ann Biomed Eng 41:1049–1061. doi:10.1007/s10439-013-0755-0

28. Töger J, Kanski M, Carlsson M et al (2012) Vortex ring formation in the left ventricle of the heart: analysis by 4D flow MRI and Lagrangian coherent structures. Ann Biomed Eng 40:2652–2662. doi:10.1007/s10439-012-0615-3

29. Pierrehumbert RT (1991) Large-scale horizontal mixing in planetary atmospheres. Phys Fluids A Fluid Dyn (1989–1993) 3:1250–1260. doi:10.1063/1.858053

30. Liu M, Muzzio FJ, Peskin RL (1994) Quantification of mixing in aperiodic chaotic flows. Chaos Solitons Fractals 4:869–893. doi:10.1016/0960-0779(94)90129-5

31. Fadlun EA, Verzicco R, Orlandi P, Mohd-Yusof J (2000) Combined immersed-boundary finite-difference methods for three-dimensional complex flow simulations. J Comput Phys 161:35–60. doi:10.1006/jcph.2000.6484

32. Domenichini F (2008) On the consistency of the direct forcing method in the fractional step solution of the Navier–Stokes equations. J Comput Phys 227:6372–6384. doi:10.1016/j.jcp.2008.03.009

33. Domenichini F, Pedrizzetti G (2011) Intraventricular vortex flow changes in the infarcted left ventricle: numerical results in an idealised 3D shape. Comput Methods Biomech Biomed Eng 14:95–101. doi:10.1080/10255842.2010.485987

34. Haller G, Yuan G (2000) Lagrangian coherent structures and mixing in two-dimensional turbulence. Phys D 147:352–370. doi:10.1016/S0167-2789(00)00142-1

35. Haller G (2001) Distinguished material surfaces and coherent structures in three-dimensional fluid flows. Phys D 149:248–277. doi:10.1016/S0167-2789(00)00199-8

36. du Toit PC, Marsden JE (2010) Horseshoes in hurricanes. J fixed point theory appl 7:351–384. doi:10.1007/s11784-010-0028-6

37. Eberly D, Gardner R, Morse B et al (1994) Ridges for image analysis. J Math Imaging Vis 4:353–373. doi:10.1007/BF01262402

38. Haller G (2011) A variational theory of hyperbolic Lagrangian coherent structures. Phys D 240:574–598. doi:10.1016/j.physd.2010.11.010

39. Farazmand M, Haller G (2012) Computing Lagrangian coherent structures from their variational theory. Chaos Interdiscip J Nonlinear Sci 22:013128. doi:10.1063/1.3690153

40. Schultz T, Theisel H, Seidel H-P (2010) Crease surfaces: from theory to extraction and application to diffusion tensor MRI. IEEE Trans Vis Comput Gr 16:109–119. doi:10.1109/TVCG.2009.44

41. Mangual JO, Domenichini F, Pedrizzetti G (2012) Describing the highly three dimensional right ventricle flow. Ann Biomed Eng 40:1790–1801. doi:10.1007/s10439-012-0540-5

42. Fortini S, Querzoli G, Espa S, Cenedese A (2013) Three-dimensional structure of the flow inside the left ventricle of the human heart. Exp Fluids 54:1–9. doi:10.1007/s00348-013-1609-0

43. Elbaz MSM, Calkoen EE, Westenberg JJM et al (2014) Vortex flow during early and late left ventricular filling in normal subjects: quantitative characterization using retrospectively-gated 4D flow cardiovascular magnetic resonance and three-dimensional vortex core analysis. J Cardiovasc Magn Reson 16:78. doi:10.1186/s12968-014-0078-9

44. Beron-Vera FJ, Olascoaga MJ, Goni GJ (2010) Surface ocean mixing inferred from different multisatellite altimetry measurements. J Phys Oceanogr 40:2466–2480. doi:10.1175/2010JPO4458.1